Bioelectrochemistry 144 (2022) 108049

Contents lists available at ScienceDirect

Bioelectrochemistry

journal homepage: www.elsevier.com/locate/bioelechem

Involvement of $O_2^{\cdot-}$ release in zearalenone-induced hormesis of intestinal porcine enterocytes: An electrochemical sensor-based analysis

Yanjing Yun [a,b], Zhisong Lu [a,b,*], Xiaodan Jiao [a,b], Peng Xue [a,b], Wei Sun [c], Yan Qiao [a,b,*], Yang Liu [d,*]

[a] Key Laboratory of Luminescence Analysis and Molecular Sensing (Southwest University), Ministry of Education, School of Materials & Energy, Southwest University, No. 1 Tiansheng Road, Chongqing 400715, PR China
[b] Institute for Clean Energy & Advanced Materials, School of Materials & Energy, Southwest University, No.1 Tiansheng Road, Chongqing 400715, PR China
[c] Key Laboratory of Laser Technology and Optoelectronic Functional Materials of Hainan Province, College of Chemistry and Chemical Engineering, Hainan Normal University, Haikou 571158, PR China
[d] School of Food Science and Engineering, Foshan University/Quality Control Technical Center (Foshan) of National Famous and Special Agricultural Products (CAQS—GAP—KZZX043), Foshan 528231, Guangdong, PR China

ARTICLE INFO

Article history:
Received 20 October 2021
Received in revised form 19 December 2021
Accepted 30 December 2021
Available online 4 January 2022

Keywords:
Zearalenone
Hormesis
Superoxide anion
Electrochemical method
Biosensor

ABSTRACT

Relationship between mycotoxin-induced hormesis and reactive oxygen species (ROS) has not been systematically investigated due to the lack of an effective analysis method. To monitor cellular release and intracellular level of $O_2^{\cdot-}$, carboxymethyl cellulose-$Mn_3(PO_4)_2$ nanocomposite was synthesized to fabricate an electrochemical biosensor, which selectively detects $O_2^{\cdot-}$ over the range of 57.50 nM ~ 2.95 μM (R^2 = 0.99) with the sensitivity of 78.67 μA μM^{-1} cm^{-2} and the detection limit of 8.47 nM. Transient exposure to zearalenone (ZEA) induces the enhancement on cell viability, immediate $O_2^{\cdot-}$ release from cells, and reduction of intracellular $O_2^{\cdot-}$ level. After post-treatment culture, intracellular $O_2^{\cdot-}$ initially increases to a high level and then decreases to the normal level. Concurrently, the ZEA-induced hormesis disappears. Based on the findings, we propose a mechanism, involving the ROS release, increase of succinate dehydrogenase activity and recovery of intracellular ROS, to explain the occurrence and disappearance of hormesis in intestinal porcine enterocytes.

1. Introduction

Mycotoxins are a class of secondary metabolites of filamentous fungi, which exert adverse health effects in humans and animals [1]. Due to their capability to induce carcinogenesis, teratogenicity, mutagenicity, cytotoxicity, nephrotoxicity, hepatotoxicity and immunotoxicity, mycotoxins have been regarded as worldwide food contaminants. Hormesis, a generally accepted biological phenomenon in the field of toxicology, refers to a biphasic dose–response that defined as low-dose stimulation and high-dose inhibition [2]. The phenomenon has been reported in mycotoxin-induced biological effects. The proliferation of splenic cells was significantly reduced in chickens fed with diets containing 10 mg kg^{-1} of deoxynivalenol (DON), but low levels (2 and 5 mg kg^{-1}) of DON could promote the cell proliferation [3]. Typical hormetic effects on the body weight have been observed in chickens fed with diets containing graded levels of aflatoxins. In comparison to the high-dose aflatoxins caused weight loss, broiler chickens receiving 625 and 1250 μg kg^{-1} dietary total aflatoxins showed 3.3% and 1.0% improvements in the body weight, respectively [4]. Huff *et al.* also found that diet containing 1250 μg kg^{-1} of total aflatoxins stimulated a 7.1% increase in the chicken body weight. However, 2500 and 5000 μg kg^{-1} of aflatoxins in the diet resulted in 89.2 and 77.1% decreases in body weight, respectively [5].

Zearalenone (ZEA) is a non-steroid mycotoxin produced by several Fusarium species [6]. It often contaminates cereals, fruits and vegetables, further causing functional and morphological alteration in reproductive organs [7]. ZEA also exhibits hepatotoxicity, hematotoxicity, immunotoxicity and genotoxicity [8]. Low doses of ZEA could generate stimulating/adaptive effects in female Beagle dogs, accelerating somatic growth and increasing body weight [9]. The dose–response curves of ZEA-induced cytotoxicity of KK-1 cells displayed a hormetic shape with the stimulation peak value of 60% [10]. After reviewing the literatures on pre-pubertal female dogs exposed to ZEA, Gajęcka *et al.* proposed that low doses of ZEA could improve ovarian and uterine function, whereas higher doses were toxic [11]. Although ZEA-induced hormetic bio-effects have already been verified, the relationship between ZEA exposure

* Corresponding authors.
E-mail addresses: zslu@swu.edu.cn (Z. Lu), yanqiao@swu.edu.cn (Y. Qiao), liuyang@fosu.edu.cn (Y. Liu).

https://doi.org/10.1016/j.bioelechem.2021.108049
1567-5394/

duration and hormesis responses, as well as the corresponding mechanism, have not been thoroughly investigated.

A few hypotheses have been proposed to explain the hormesis phenomenon, including oxidative stress-involved, overcompensation-based, receptor-mediated, and signaling-mediated mechanisms [12–14]. Among them, oxidative stress-involved mechanism is the most attractive one. A large amount of evidences have proven that a low level of reactive oxygen species (ROS) could improve systemic defense by inducing an adaptive response [15]. It was reported that small amount (50 mg L^{-1}) of sulfonated graphene reduced the ROS level, further stimulating the plant growth. But, at a higher concentration (500 mg L^{-1}), the plant height was inhibited [16,17]. A low concentration of ROS generated by mitochondria might act as signaling molecules to promote the changes of cellular defense system and mitochondrial dynamics, resulting in extended lifespan [18]. Therefore, it is of great importance to analyze ROS changes during the mycotoxin-exposure process for better understanding the mycotoxin-induced hormesis.

ROS are by-products of the aerobic metabolism, consisting of superoxide anion ($O_2^{\cdot-}$), hydrogen peroxide (H_2O_2), and hydroxyl radicals (OH·) [19]. Real-time monitoring of ROS is extremely difficult because of their very short half-life. Currently, ROS are mainly measured with fluorescence spectrophotometry, chemiluminescence, electron spin resonance trapping, and chromatography [20]. These technologies could provide satisfied accuracy and sensitivity, but well-trained professionals, tedious operation procedures, and expensive instruments are usually needed. More importantly, those methods could not real-time monitor the instant state of intracellular ROS and the ROS secreted from living cells. Electrochemical methods have been applied to measure ROS secreted from living cells due to their easy operation, real-time sensing, high sensitivity, and fast response [21–24]. Since enzymes such as superoxide dismutase (SOD) and cytochrome *c* possess excellent specificity and catalytic capability towards $O_2^{\cdot-}$, they have been widely utilized as recognition components to prepare electrochemical $O_2^{\cdot-}$ sensors. However, the application of the enzyme-based electrochemical biosensors is greatly limited by high cost, short lifespan, and poor repeatability. $Mn_3(PO_4)_2$ can function as an effective mimetic enzyme to catalyze dismutation of $O_2^{\cdot-}$ [25]. Its combination with carboxymethyl cellulose (CMC) might provide both good catalytic activity towards $O_2^{\cdot-}$ and biocompatible surface for the attachment of living cells. Therefore, as shown in Scheme 1, CMC–$Mn_3(PO_4)_2$ was synthesized to fabricate an electrochemical sensor for real-time monitoring $O_2^{\cdot-}$ released from the living cells. ZEA was employed to treat living cells for the construction of hormetic cell model, in which the cell viability was measured to reflect the biological responses. During the transient exposure process, ZEA-trigged $O_2^{\cdot-}$ release from living cells and the total $O_2^{\cdot-}$ in the cells were monitored with the as-prepared electrochemical sensors, respectively, to reveal the possible role of ROS in ZEA-induced hormesis.

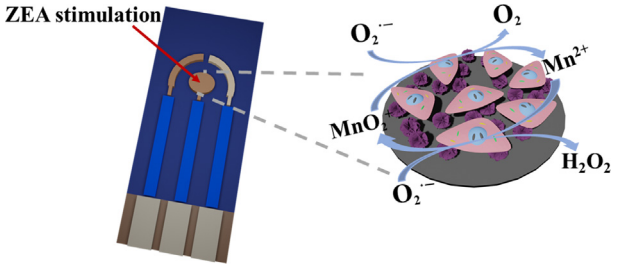

Scheme 1. Schematic diagram of the CMC–$Mn_3(PO_4)_2$-based electrochemical sensor.

2. Experimental procedures

2.1. Chemicals

CMC, manganese sulfate monohydrate ($MnSO_4{\cdot}H_2O$, 99.99%), potassium phosphate tribasic (K_3PO_4, ACS), potassium superoxide (KO_2, 96.5%), potassium chloride (KCl, 99.8%), sodium nitrate ($NaNO_3$, ≥99.0%), uric acid (UA, 99%), ascorbic acid (AA, 99%), dopamine hydrochloride (DA, 98%) and hydrogen peroxide (H_2O_2, 30%) were purchased from Aladdin Bio-Chemistry Technology Co., Ltd (P. R. China). Nafion (5 wt% in ethanol), zymosan A (Zym, from Saccharomyces cerevisiae), 2′,7′– dichlorodihydrofluorescein diacetate (DCFH–DA), thiazolyl blue tetrazolium bromide (MTT, 98%) and dimethyl sulfoxide (DMSO) were brought from Sigma–Aldrich (Shanghai, China). ZEA (≥98%) was obtained from Cayman Chemical Company (USA). RIPA lysis buffer was purchased from Beyotime Biotechnology (China). Intestinal Porcine Epithelial Cell line-J2 (IPEC-J2) was purchased from Nanjing Herb Source Bio-Technology Co., Ltd (Nanjing, China). Formulated Dulbecco's modified eagle's medium (DMEM), fetal bovine serum (FBS), TrypLE™ express enzyme and phosphate-buffered saline (PBS) were produced by Thermo Fisher Scientific (USA). Other chemicals were of analytical grade and used without further purification.

2.2. Preparation of $Mn_3(PO_4)_2$ and CMC–$Mn_3(PO_4)_2$

CMC–$Mn_3(PO_4)_2$ composites were synthesized according to Wang's method with minor modifications [26]. Initially, 26.44 mg CMC was fully dissolved in 20 mL water, followed by the addition of 5 mL of $MnSO_4$ (0.12 M) under constant stirring for 4 h. Then, 5 mL of K_3PO_4 (0.08 M) was introduced in the mixture, stirring consecutively under ice bath. During this process, white-colored precipitates appeared in the solution. Finally, the pellets were washed with water under centrifugation (10,000 rpm for 10 min) for 3 times. The final products were freeze-dried and stored at ambient conditions for further usage. Pristine $Mn_3(PO_4)_2$ was prepared with the same procedures without the addition of CMC.

2.3. Electrochemical measurement

Electrochemical measurements were conducted with a CHI 660D electrochemical workstation (CH Instruments, Shanghai, China). Electrocatalytic behavior of CMC–$Mn_3(PO_4)_2$ towards $O_2^{\cdot-}$ was investigated by cyclic voltammetry (CV) at a scan rate of 50 mV s^{-1}. In order to investigate the sensing performance, different amount of $O_2^{\cdot-}$ was added into PBS under stirring to measure the detection range and sensitivity. $NaNO_3$, KCl, DA, AA, and H_2O_2 were selected as interfering species to carry out the interference assay.

2.4. Fabrication of modified electrode

Screen-printed carbon electrodes (SPCE) were commercially purchased from Yancheng Dejing Technology Co. Ltd (P. R. China). The as-prepared CMC–$Mn_3(PO_4)_2$ or $Mn_3(PO_4)_2$ powder was suspended in water to obtain a 10 mg mL^{-1} suspension. Then, 1 μL of the above suspension was deposited on the surface of SPCE, drying at room temperature. Two microliter of 1% Nafion ethanol solution was dropped onto the electrode surface to obtain a uniform thin film. Finally, a home-made reaction chamber with the diameter of ~ 1.80 cm was fixed on the electrode to hold the electrolyte solution during the measurement. Before cell seeding and culture, the as-prepared electrode was sterilized with UV light for 30 min.

2.5. Cell fixation

The electrode-attached cells were fixed with 4% paraformaldehyde for 30 min, followed by the successive dehydration with gradient ethanol solutions. Then, the samples were freeze–dried and directly utilized for field emission scanning electron microscopy (FESEM).

2.6. Electrochemical measurements of extracellular and intracellular $O_2^{\cdot-}$

Measurement of extracellular $O_2^{\cdot-}$. IPEC–J2 cells were cultured on the modified SPCE at 37 ℃ for 12 h. After that, the culture medium was removed and 0.01 M PBS was added into the reaction chamber as the electrolyte. ZEA (100 μM) was employed to stimulate the release of $O_2^{\cdot-}$ from the living cells. The current responses were real-time recorded with chronoamperometry method.

Measurement of intracellular $O_2^{\cdot-}$. IPEC–J2 cells were seeded in a 12–well plate at a density of 6×10^4 cells per well, culturing at 37 ℃ overnight. ZEA was applied to stimulate the cells for 2 min, followed by 0.01 M PBS washing for three times. After an incubation under culture conditions for different durations, the cells were collected from the plates and re-suspended in 0.01 M PBS to achieve a cell density of 3×10^5 cells mL^{-1}. The cell suspension (100 μL) was mixed with the RIPA buffer to lyse the cells for the release of intracellular $O_2^{\cdot-}$.

2.7. Cell viability assay

The cell viability was evaluated with the MTT cell proliferation/viability assay kit. Briefly, cells were cultured in 96–well plates (1×10^4 cells per well) at 37 ℃ overnight and further treated with ZEA for different durations. After rinsing with PBS, the cells were incubated with the MTT solution (100 μL, 0.5 mg mL^{-1}) for 4 h. Then, DMSO (200 μL) was utilized to dissolve the purple precipitates under gently shaking for 15 min. Absorbance intensity at 570 nm was measured by a microplate reader (SPARK 10 M, TECAN, Swizerland). Viabilities of the cells recovered from ZEA stimulation were measured with the same method, respectively. The relative cell viability was calculated with the following equation:

$$\text{Cell viability}(\%) = \frac{Abs570\ of\ treated\ cells}{Abs570\ of\ control\ cells} \times 100\%$$

3. Results and discussion

3.1. Characterization of CMC–$Mn_3(PO_4)_2$ nanocomposites

FESEM was used to characterize morphologies of the as-prepared CMC, $Mn_3(PO_4)_2$ and CMC–$Mn_3(PO_4)_2$. CMC exhibits a fiber shape with the length of ~ 200 μm and width of ~ 20 μm (Fig. S1(a) in ESI). In the aqueous system without CMC, $Mn_3(PO_4)_2$ agglomerates easily to form micron-scale sheet structures (Fig. 1a). With the addition of CMC, the products display spherical flower-like structures, indicating the formation of CMC–$Mn_3(PO_4)_2$ nanocomposites. From the enlarged SEM image, it can be observed that nanosheets with thickness of a few nanometers form the petals of each flower (Fig. 1b). TEM image further illustrates that nanofibers are embedded in the nanosheet to support the structures (Fig. 1c). Regular lattice fringes in the high-resolution TEM image show the good crystalline structure of $Mn_3(PO_4)_2$ in the nanosheets (Fig. 1d). P, O, Mn and C elements are uniformly distributed in nanoflowers, further proving that the synthesized materials are CMC–$Mn_3(PO_4)_2$ nanocomposites (Fig. S1(b) in ESI). The successful synthesis of CMC–$Mn_3(PO_4)_2$ nanocomposites were also verified by measuring the zeta potentials (Fig. S2 in ESI). The zeta potential of CMC is –46 ± 0.85 mV, which is mainly attributed to the presence of a large number of carboxyl groups and oxygen-containing groups on the CMC surface. After addition of Mn precursors, the zeta potential increases to –5.40 ± 0.81 mV due to the adsorption of Mn ions. As to the CMC–$Mn_3(PO_4)_2$ nanocomposites, the zeta potential changes to –19.77 ± 0.15 mV due to the bonding of negatively charged phosphate radical group.

The X-ray diffraction peaks of CMC–$Mn_3(PO_4)_2$ match well with the standard JCPDS card (No. 03–0426), verifying the existence of $Mn_3(PO_4)_2$ crystals in the composites (Fig. 1e). X-ray photoelectron spectroscopy was used to explore surface chemical state and structural details of the composites. The characteristic peaks of C 1s, O 1s, Mn 2p and P 2p are observed at 284.8, 530.4, 640.5 and 131.9 eV, respectively. The C 1s peak can be divided into three prominent peaks at 284.8, 286.5, and 288.0 eV, attributing to C=C, C–O, and O–C=O, respectively (Fig. S3a in ESI). The Mn 2p spectrum (Fig. S3b in ESI) possesses two major peaks at 641.8 eV and 653.5 eV, corresponding to Mn 2p 3/2 and Mn 2p 1/2, respectively. The weak peak at 645.8 eV could be assigned to MnO, indicating the presence of MnO in CMC–$Mn_3(PO_4)_2$ nanocomposites [27]. A typical peak of P 2p could be observed in Fig. S3c, corresponding to PO_4^{3-} [28]. The data prove that CMC–$Mn_3(PO_4)_2$ nanocomposites with flower-structures and good crystallinity were successfully synthesized in the present work.

3.2. Characterization of CMC–$Mn_3(PO_4)_2$ nanocomposite-based electrochemical $O_2^{\cdot-}$ sensor

The CMC–$Mn_3(PO_4)_2$ nanocomposites were immobilized on SPCE to fabricate the $O_2^{\cdot-}$electrochemical sensor. CVs were measured to investigate the electrochemical behavior of the materials at a scan rate of 50 mV s^{-1} in 0.1 M PBS (pH = 7.4). As shown in Fig. 2a, no redox peaks appear for the bare electrode, but CMC–$Mn_3(PO_4)_2$ composite-modified one exhibits a pair of wide redox peaks in the range of 0.6–0.8 V and 0.2–0.5 V in the absence of $O_2^{\cdot-}$, respectively, which can be caused by the electrochemical transformation between Mn (II) and Mn (III) [29]. In the presence of $O_2^{\cdot-}$, both peaks remarkably increase, which could be attributed to the oxidation and reduction towards $O_2^{\cdot-}$, respectively. Specifically, during the redox process one $O_2^{\cdot-}$ oxidizes the Mn^{2+} to generate MnO_2^+ and H_2O_2, while another $O_2^{\cdot-}$ simultaneously reduces the MnO_2^+ to produce Mn^{2+} and O_2 [30]. Although the $Mn_3(PO_4)_2$ electrode also has corresponding redox peaks, its response towards $O_2^{\cdot-}$ is not quite obvious. The results demonstrate that the CMC–$Mn_3(PO_4)_2$ nanocomposite possesses great electrocatalytic activity to catalyze the electrochemical oxidation of $O_2^{\cdot-}$ on the electrode surface.

To understand the catalytic process, CV curves were collected at the scan rate ranging from 20 to 140 mV s^{-1}(Fig. S4 in ESI). With the increase of the scan rate, the anodic peak current linearly enhances (R^2 = 0.99), suggesting a surface-controlled fast process towards $O_2^{\cdot-}$ oxidation. To further study the response of the electrochemical sensor, a steady-state current–time curve was recorded at an applied potential of 0.75 V in 0.1 M PBS (pH 7.4) under gentle stirring (Fig. 2b). Addition of 57.50 nM $O_2^{\cdot-}$ could induce a distinct current response. With the successive addition of $O_2^{\cdot-}$, the current exhibits a stepped enhancement until the $O_2^{\cdot-}$ concentration reaches to 2.95 μM. The corresponding calibration curve exhibits a linear dynamic range from 57.50 nM to 2.95 μM with the detection limit of 8.47 nM and the sensitivity of 78.67 μA μM^{-1} cm^{-2} (Fig. 2c). The LOD was determined with the formula: LOD = $3\sigma/S$, where σ is the standard deviation of negative control, S is the slope of calibration curve. In comparison to the reported $O_2^{\cdot-}$ biosensors (Table S1 in ESI), the as-prepared sen-

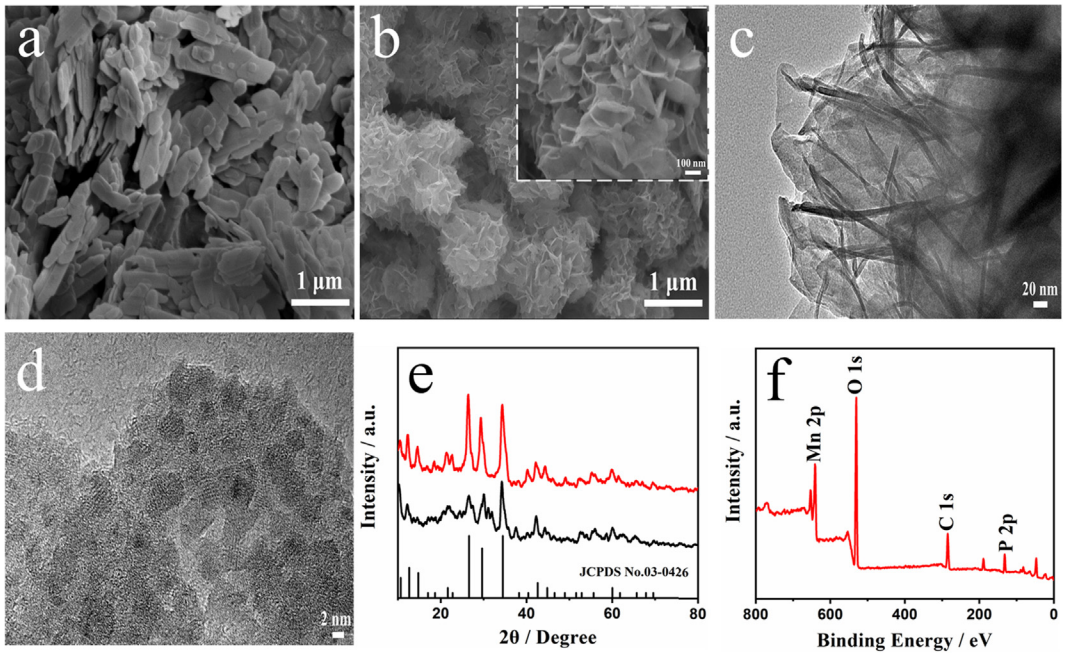

Fig. 1. (a) FESEM image of $Mn_3(PO_4)_2$; (b) FESEM image of CMC–$Mn_3(PO_4)_2$ nanocomposites; (c, d) TEM images of CMC–$Mn_3(PO_4)_2$ nanocomposites; (e) XRD patterns of $Mn_3(PO_4)_2$ (black line) and CMC–$Mn_3(PO_4)_2$ (red line); (f) XPS spectra of CMC–$Mn_3(PO_4)_2$ nanocomposites. (For interpretation of the references to colour in this figure legend, the reader is referred to the web version of this article.)

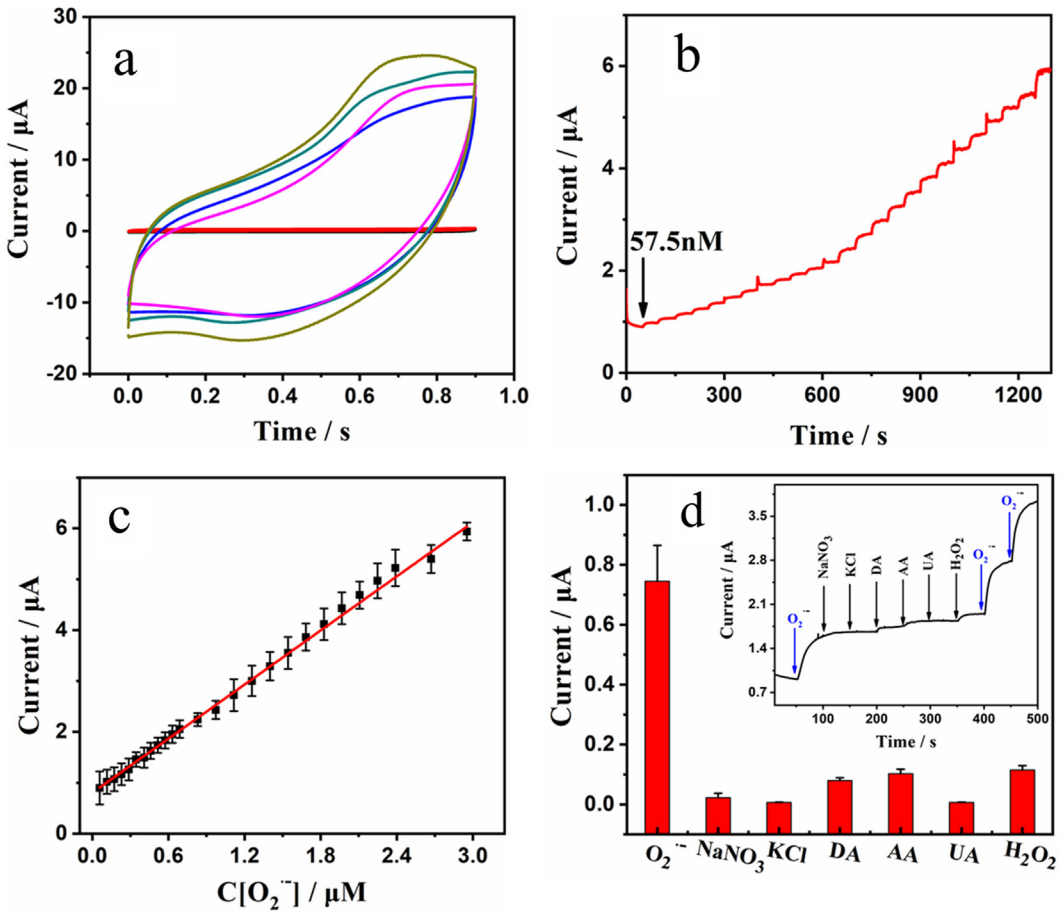

Fig. 2. (a) Cyclic voltammetry curves of the bare (black line), CMC (red line), $Mn_3(PO_4)_2$ (blue line) and CMC–$Mn_3(PO_4)_2$ (pink line) electrodes in the absence of 1 μM $O_2^{\cdot-}$ and CV curves of the $Mn_3(PO_4)_2$ (dark cyan line) and CMC–$Mn_3(PO_4)_2$ (dark yellow line) in the presence of 1 μM $O_2^{\cdot-}$; Chronoamperometric responses (b) and linear calibration curve (c) of CMC–$Mn_3(PO_4)_2$ nanocomposite-based sensors upon continuous addition of different concentrations of $O_2^{\cdot-}$ at an applied potential of 0.75 V in 0.1 M PBS, with the linear equation: y = 1.77x + 0.80 (R^2 = 0.99); (d) Selectivity of the CMC–$Mn_3(PO_4)_2$ nanocomposite-based sensor. (For interpretation of the references to colour in this figure legend, the reader is referred to the web version of this article.)

sor shows higher sensitivity, which is conducive to the detection of $O_2^{\cdot-}$ in complex real samples, in particular biological systems containing living cells.

Previous studies have confirmed that H_2O_2 is also a kind of reactive oxygen species [31]. Moreover, there are various small molecules or ions in living systems. Therefore, in order to investigate the anti-interference capability, $O_2^{\cdot-}$ (1 μM), $NaNO_3$ (10 μM), KCl (10 μM), DA (10 μM), AA (10 μM), and H_2O_2 (10 μM) were successively added into 0.1 M PBS (pH 7.4). In contrast to the remarkable responses to $O_2^{\cdot-}$, the sensor does not respond to any of the interferences (Fig. 2d). The results indicate that the sensor has excellent selectivity. Fig. S5a shows the current responses of three independent CMC–$Mn_3(PO_4)_2$-modified electrodes to 1 μM $O_2^{\cdot-}$, indicating the great reproducibility of the sensor.

3.3. Hormesis cell model and ZEA-triggered $O_2^{\cdot-}$ release from cells

To evaluate the dose effect of ZEA in the short-term stimulation, IPEC-J2 cells were stimulated with 0, 25, 100 and 200 μM of ZEA for 2 min (Fig. 3a), respectively. Based on data obtained from the MTT assay, the cell viability significantly enhances in all ZEA-treated groups, which is quite distinct from the cytotoxic effects-caused by long-term exposure (more than 12 h) of ZEA [32]. The increase of the cell viability could be defined as the ZEA-induced hormesis under a transient exposure [15]. Since ZEA-induced increase of cell viability reaches plateau at the concentration of 100 μM, 100 μM is selected as the optimal concentration to construct the hormesis cell model induced by transient ZEA exposure. In order to further investigate the effect of the exposure duration on the hormesis, the cells were treated with 100 μM ZEA for different time. As shown in Fig. 3b, 2 min and 1 h stimulation could induce significant enhancement on the cell viability. However, after 2 h of ZEA exposure, the hormetic response disappears. Moreover, the cell viability sharply decreases after 3 h, indicating the toxic effects of ZEA on the cells. The results suggest that 100 μM ZEA can lead to hormetic response on cell viability in a time-dependent manner, which agrees well with the findings in short-term exposure of microbes to antibiotics or chemical mixtures [33,34]. Oxidative stress has been widely accepted as the major mechanism for mycotoxin-caused cytotoxicity [35]. The alteration of intracellulr ROS has also been investigated to explain the hormetic bioeffects in toxin-treated cells [36]. Thus, the as-prepared electrochemical sensor was employed to explore the role of $O_2^{\cdot-}$ in the time-dependent hormesis of ZEA.

The IPEC-J2 cells were cultured on the nanocomposite-functionalized SPCE before the ZEA treatment (Fig. S6 in ESI). Because of the biocompatibility of CMC, the cells could be efficiently attached on the modified electrode surface (Fig. 3c). Fig. S7a in ESI shows the gradual reduction of peak current and continuous increase of the peak separation with the successive modification of CMC-$Mn_3(PO_4)_2$ and cells on the SPCE. The smallest semicircle in the Nyquist plots also indicate the same trend. The

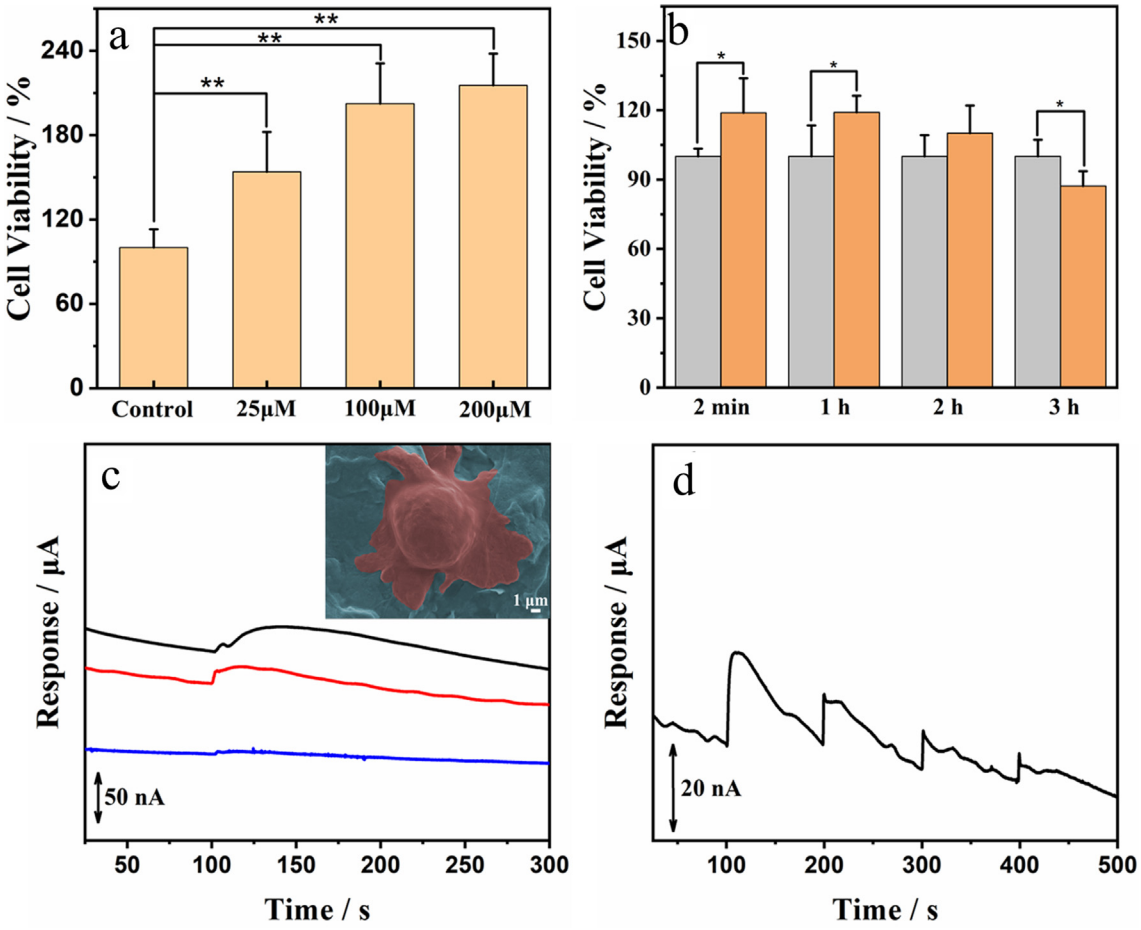

Fig. 3. (a) Cell viability after treatment with different concentrations of ZEA for 2 min; (b) Cell viability after treatment with 0.01 M PBS (gray column) and 100 μM ZEA (brown column) for different time; (c) Real-time monitoring of $O_2^{\cdot-}$ released from IPEC-J2 cells stimulated by 100 μM ZEA (black line), 0.1 mg mL^{-1} Zym (red line) and 0.01 M PBS (blue line) at an applied potential of 0.75 V (Inset: morphology of the cells on the CMC–$Mn_3(PO_4)_2$ electrode); (d) Real-time monitoring of $O_2^{\cdot-}$ released from IPEC-J2 cells upon continuous addition of 100 μM ZEA at an applied potential of 0.75 V. (For interpretation of the references to colour in this figure legend, the reader is referred to the web version of this article.)

shift of EIS diagram can be attributed to the attachment of insulated cells (Fig. S7b in ESI). The results verify the successful immobilization of the nanocomposites and efficient attachment of the cells. Zymosan (Zym) was widely utilized as a stimulating agent to induce the release of $O_2^{\cdot-}$ from living cells [37]. Addition of 0.1 mg mL^{-1} Zym in the system leads to a significant enhancement on the current (Fig. 3c), showing that the Zym-triggered release of $O_2^{\cdot-}$ could be efficiently detected with the as-prepared biosensors. In comparison to the negligible change in the PBS solvent group, injection of 100 μM ZEA could induce an obvious current peak in the curve, which could be attributed to the response of the biosensor towards ZEA-triggered release of $O_2^{\cdot-}$ from the cells [20]. Interestingly, the current generated by the first-time ZEA stimulus is always the highest (Fig. 3d). Whereas, the signals upon 2nd, 3rd and 4th addition of ZEA (100 μM) continuously decrease, suggesting that ZEA-triggered release of $O_2^{\cdot-}$ is not a dose-dependent process and the recovery of intracellular $O_2^{\cdot-}$ may take time [38,39]. ROS are not only by-product of cellular metabolism, but also critical signal molecules [40]. Imbalance between intracellular oxidative and anti-oxidative systems is deemed as an important mechanism for toxin-induced hormesis [41]. A small amount of carbon nanotubes and metal nanoparticles could remove ROS in plants, thereby reducing oxidative stress and promoting plant growth [16,42]. Therefore, the ZEA-triggered release of $O_2^{\cdot-}$ may also result in the reduction of intracellular ROS level, further initiating the enhancement of cell viability as shown in Fig. 3a.

3.4. Recovery of intracellular $O_2^{\cdot-}$ after ZEA transient exposure

In order to investigate change and recovery of intracellular $O_2^{\cdot-}$ after ZEA transient exposure, the cells were decomposed with the RIPA lysis buffer to free intracellular $O_2^{\cdot-}$ into the detection system for electrochemical sensing. As shown in Fig. 4a, for the control group, the peak value of the current response is 1209 nA, which is significantly higher than that in the ZEA-treated one (1077 nA). That could be attributed to the release of $O_2^{\cdot-}$ upon 100 μM ZEA stimulation, being consistent with the data in Fig. 3c. The negligible response of the system without cells could rule out the possible interference of the RIPA buffer. The cells transiently exposed to ZEA were washed with PBS and further cultured for 1, 2 and 4 h, respectively. The intracellular $O_2^{\cdot-}$ levels were measured with the lysis buffer-assisted electrochemical sensing approach. After 1 h incubation, the current peak of the ZEA-treated group is much higher than that of the control cells (Fig. 4b). As the time extends to 2 h, the peak current value in the experimental group is still higher than that in the control group, but the gap between the two groups reduces (Fig. 4c). Interestingly, after 4 h culture, there is no significant difference on the peak current between the treated and the control groups (Fig. 4d). The results reveal that the intracellular $O_2^{\cdot-}$ firstly increases to a high level and then decreases to the normal level during the post-treatment culture process. This trend is also verified with the intracellular ROS fluorescent tests based on DCFH-DA probe (Fig. S8 in ESI). Cell is a complicated bio-

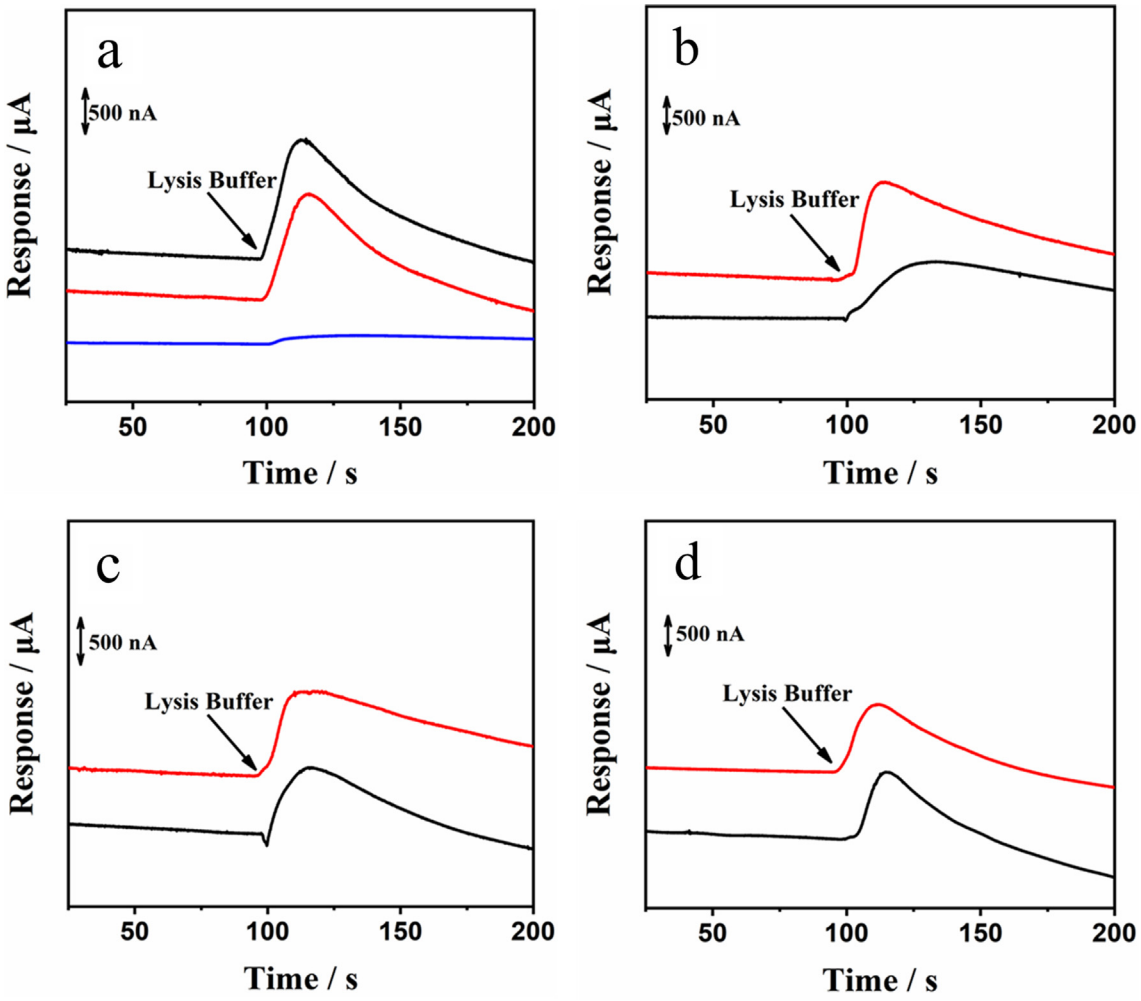

Fig. 4. Real-time monitoring of $O_2^{\cdot-}$ released from PBS (blue line) and the lysed cells that were pretreated with 100 μM ZEA (red line) and 0.01 M PBS (black line) for 2 min, respectively, and then cultured for 0 (a), 1 (b), 2 (c) and 4 (d) h. (For interpretation of the references to colour in this figure legend, the reader is referred to the web version of this article.)

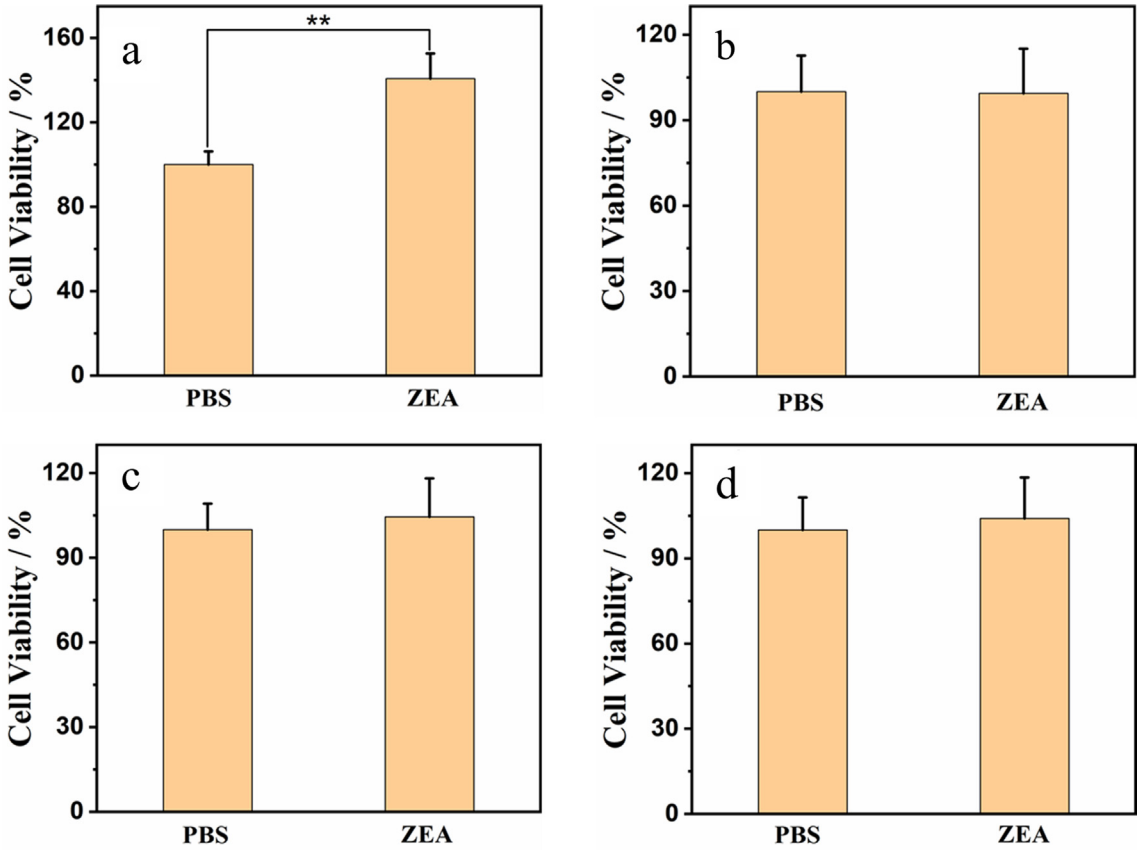

Fig. 5. Cell viability of ZEA-pretreated IPEC-J2 cells after 0 (a), 1 (b), 2 (c), 4 (d) h of culture in normal conditions.

logical system with evolutionary self-repair capability. Once the oxidative/anti-oxidative balance is broken by ZEA stimulation, the cell may initiate its repair system to top up the intracellular ROS. The much higher $O_2^{\cdot-}$ level in the cells at 1 h may be caused by the "over-compensation" effects, but after a relative long-term culture, the intracellular $O_2^{\cdot-}$ eventually goes back to the normal level.

3.5. Cell viability after recovery of intracellular $O_2^{\cdot-}$

The ZEA-triggered release of $O_2^{\cdot-}$ and further reduction of intracellular $O_2^{\cdot-}$ level have been proven with the as-prepared electrochemical sensor. Based on the literatures and the above findings, it can be speculated that the decrease of intracellular $O_2^{\cdot-}$ level may contribute to the transient ZEA stimulation-induced hormetic effects on the cell viability. In Fig. 4, we observed that intracellular $O_2^{\cdot-}$ could recover to the normal level after 4 h's post-treatment culture. To further verify the relationship between intracellular $O_2^{\cdot-}$ and the ZEA-induced hormesis, cell viability of ZEA-pretreated IPEC-J2 cells were measured after 0, 1, 2 and 4 h of culture (Fig. 5). The cells without post-treatment culture show the enhanced viability, which is consistent with the results in above experiments. However, after 1–4 h's culture, no significant difference on the cell viability could be observed between the control and ZEA-stimulated groups. As being discussed in above section, the ZEA-treated cells could initiate the repair systems and recover the intracellular $O_2^{\cdot-}$ level. Thus, the disappearance of the ZEA-induced hormetic bio-effects after pretreatment culture may be associated with the recovery of the intracellular $O_2^{\cdot-}$ level.

Mitochondrion is the major organelle for the generation of ROS. Moreover, the mitochondrial succinate dehydrogenase (SDH) redox activity is measured to reflect the cell viability in MTT. Thus, both ROS and SDH may be involved in the ZEA-induced hormesis. It has been reported that SDH activity is correlated to the ROS production in mitochondria [43,44]. The SDH catalyzed transform of succinate to fumarate is always accompanied by the production of $O_2^{\cdot-}$ [45]. Based on the results and literatures, we propose the following mechanism to explain ZEA-induced hormesis and its recovery process (Scheme 2): (1) the transient exposure to ZEA may trigger the release of $O_2^{\cdot-}$ from the living cells, leading to the decrease of intracellular $O_2^{\cdot-}$ level; (2) cells sense the change and initiate the repair system, in which the mitochondrial SDH activity is enhanced to accelerate the generation of endogenous $O_2^{\cdot-}$; (3) Once the intracellular $O_2^{\cdot-}$ is over-compensated, the cells slow down the $O_2^{\cdot-}$ production process; (4) Finally, the intracellular $O_2^{\cdot-}$ and mitochondrial SDH activity recovers to their normal level.

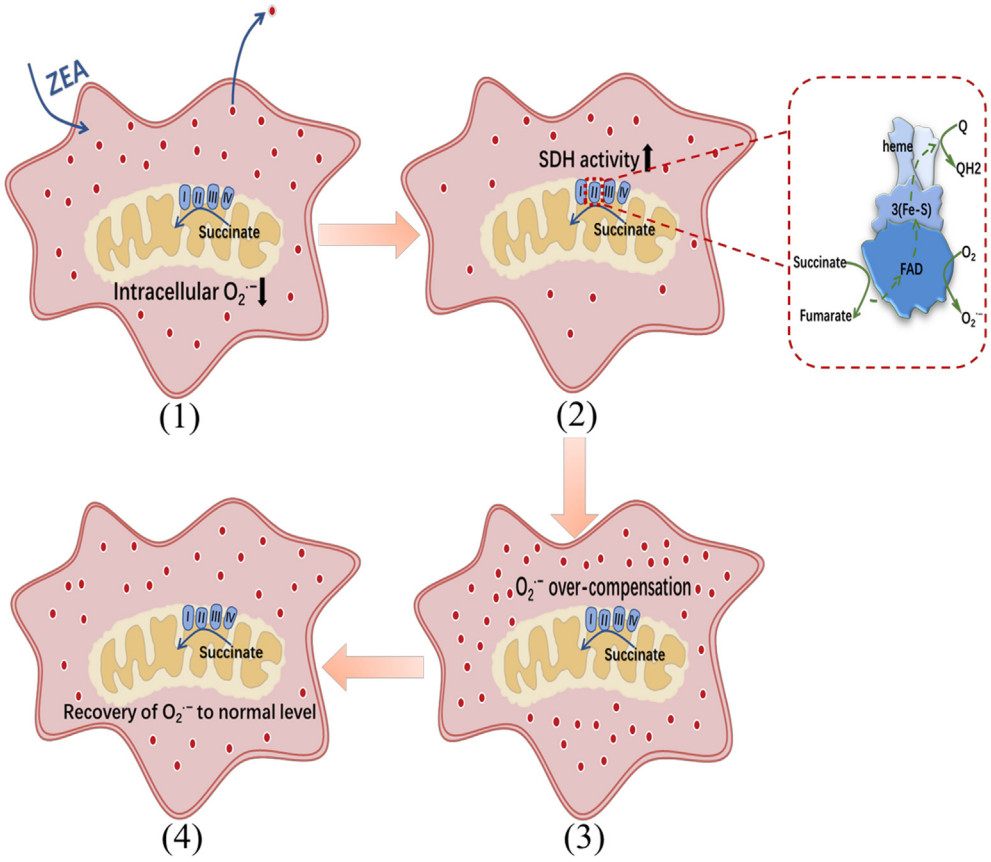

Scheme 2. Diagram of ZEA-induced hormesis and its recovery process.

4. Conclusions

In summary, CMC-$Mn_3(PO_4)_2$ nanocomposite was synthesized to prepare a sensitive $O_2^{\cdot-}$ electrochemical biosensor for investigating the possible role of $O_2^{\cdot-}$ in ZEA-induced hormesis of intestinal porcine enterocytes. The CMC and $Mn_3(PO_4)_2$ in the nanocomposite could contribute to the good biocompatibility and high catalytic activity towards $O_2^{\cdot-}$, respectively. The ZEA-induced hormesis cell model was constructed by transient exposure of IPEC-J2 cells to 100 μM ZEA. The electrochemical biosensor-based analysis reveals that transient ZEA exposure could trigger the release of $O_2^{\cdot-}$ from the living cells, leading to the reduction of intracellular ROS level. The sudden decrease of the intracellular ROS level further contributes to the hormetic effects. During the post-treatment culture process, intracellular $O_2^{\cdot-}$ initially increases to a high level and then decreases to the normal level, accompanied by the disappearance of the hormetic bio-effects. The repair system initiated by the oxidative stress may lead to the recovery of intracellular $O_2^{\cdot-}$ and cell viability. Based on the findings and literatures, we propose a possible mechanism, which successively involves ROS release, increase of SDH activity and recovery of intracellular ROS, to explain ZEA-induced hormesis and its recovery process. This work may not only advance the understanding of mycotoxin-induced hormesis, but also develop an electrochemical biosensor for the investigation of mycotoxin-caused bio-effects.

Declaration of Competing Interest

The authors declare that they have no known competing financial interests or personal relationships that could have appeared to influence the work reported in this paper.

Acknowledgments

This work was financially supported by National Key R&D Program of China (2019YFC1604500), Natural Science Foundation of Chongqing (cstc2019jcyj-msxmX0314), and Academician Station of Hainan Province (SQ2021PTZ0024).

Appendix A. Supplementary material

Supplementary data to this article can be found online at https://doi.org/10.1016/j.bioelechem.2021.108049.

References

[1] M.E.B. Da Rocha, F.D.C.O. Freire, F.E.F. Maia, M.I.F. Guedes, D. Rondina, Mycotoxins and their effects on human and animal health, Food Control 36 (2014) 159–165.
[2] E. Agathokleous, M. Kitao, E.J. Calabrese, Hormesis: highly generalizable and beyond laboratory, Trends Plant Sci. 25 (11) (2020) 1076–1086.
[3] S.S. Chen, Y.H. Li, M.F. Lin, Chronic exposure to the fusarium mycotoxin deoxynivalenol: impact on performance, immune organ, and intestinal integrity of slow-growing chickens, Toxins (Basel) 9 (2017) 334.
[4] W.E. Huff, Evaluation of tibial dyschondroplasia during aflatoxicosis and feed restriction in young broiler chickens, Poult. Sci. 59 (1980) 991–995.
[5] W.E. Huff, L.F. Kubena, R.B. Harvey, D.E. Corrier, H.H. Mollenhauer, Progression of aflatoxicosis in broiler chickens, Poult. Sci. 65 (1986) 1891–1899.
[6] A. Bertero, A. Moretti, L. Spicer, F. Caloni, Fusarium molds and mycotoxins: potential species-specific effects, Toxins (Basel) 10 (6) (2018) 244, https://doi.org/10.3390/toxins10060244.
[7] J. Fink-Gremmels, H. Malekinejad, Clinical effects and biochemical mechanisms associated with exposure to the mycoestrogen zearalenone, Anim. Feed Sci. Technol. 137 (3-4) (2007) 326–341.
[8] A. Rai, M. Das, A. Tripathi, Occurrence and toxicity of a fusarium mycotoxin, zearalenone, Crit. Rev. Food Sci. Nutr. 60 (16) (2020) 2710–2729.
[9] M. Gajecka, L. Zielonka, M. Dabrowski, M. Mroz, M. Gajecki, The effect of low doses of zearalenone and its metabolites on progesterone and 17beta-estradiol

concentrations in peripheral blood and body weights of pre-pubertal female Beagle dogs, Toxicon 76 (2013) 260–269.
[10] Y. Li, B. Zhang, X. He, W.-H. Cheng, W. Xu, Y. Luo, R. Liang, H. Luo, K. Huang, Analysis of individual and combined effects of ochratoxin A and zearalenone on HepG2 and KK-1 cells with mathematical models, Toxins (Basel) 6 (4) (2014) 1177–1192.
[11] M. Gajęcka, Ł. Zielonka, M. Gajęcki, The effect of low monotonic doses of zearalenone on selected reproductive tissues in pre-pubertal female dogs–a review, Molecules 20 (11) (2015) 20669–20687.
[12] T.V. Arumugam, M. Gleichmann, S.-C. Tang, M.P. Mattson, Hormesis/preconditioning mechanisms, the nervous system and aging, Ageing Res Rev 5 (2) (2006) 165–178.
[13] E.J. Calabrese, Hormetic mechanisms, Crit. Rev. Toxicol. 43 (7) (2013) 580–606.
[14] N. Cedergreen, Herbicides can stimulate plant growth, Weed Res. 48 (5) (2008) 429–438.
[15] M. Ristow, K. Schmeisser, Mitohormesis: promoting health and lifespan by increased levels of reactive oxygen species (ROS), Dose Response 12 (2014) 288–341.
[16] W. Ren, H. Chang, Y. Teng, Sulfonated graphene-induced hormesis is mediated through oxidative stress in the roots of maize seedlings, Sci. Total Environ. 572 (2016) 926–934.
[17] X. Zhang, W. Hu, J. Li, L. Tao, Y. Wei, A comparative study of cellular uptake and cytotoxicity of multi-walled carbon nanotubes, graphene oxide, and nanodiamond, Toxicol. Res. 1 (1) (2012) 62–68.
[18] D.F. Dai, Y.A. Chiao, D.J. Marcinek, H.H. Szeto, P.S. Rabinovitch, Mitochondrial oxidative stress in aging and healthspan, Longevity healthspan 3 (2014) 1–22.
[19] M. Schieber, N. Chandel, ROS function in redox signaling and oxidative stress, Curr. Biol. 24 (10) (2014) R453–R462.
[20] Z. Zou, X.Q. Ma, L. Zou, Z.Z. Shi, Q.Q. Sun, Q. Liu, T.T. Liang, C.M. Li, Tailoring pore structures with optimal mesopores to remarkably promote DNA adsorption guiding the growth of active $Mn_3(PO_4)_2$ toward sensitive superoxide biomimetic enzyme sensors, Nanoscale 11 (6) (2019) 2624–2630.
[21] Y. Wang, Y. Wang, F. Wang, H. Chi, G. Zhao, Y. Zhang, T. Li, Q. Wei, Electrochemical aptasensor based on gold modified thiol graphene as sensing platform and gold-palladium modified zirconium metal-organic frameworks nanozyme as signal enhancer for ultrasensitive detection of mercury ions, J. Colloid Interface Sci. 606 (2022) 510–517.
[22] Y. Wang, G. Zhao, H. Wang, Y. Zhang, N. Zhang, D. Wei, R. Feng, Q. Wei, Label-free electrochemical immunosensor based on biocompatible nanoporous Fe3O4 and biotin-streptavidin system for sensitive detection of zearalenone, Analyst 145 (2020) 1368–1375.
[23] Y. Wang, G. Zhao, G. Zhang, Y. Zhang, H. Wang, W. Cao, T. Li, Q. Wei, An electrochemical aptasensor based on gold-modified MoS_2/rGO nanocomposite and gold-palladium-modified Fe-MOFs for sensitive detection of lead ions, Sens. Actuators, B 319 (2020) 128313.
[24] Y. Tian, L. Mao, T. Okajima, T. Ohsaka, Superoxide dismutase-based third-generation biosensor for superoxide anion, Anal. Chem. 74 (2002) 2428–2434.
[25] X. Shen, Q. Wang, Y. Liu, W. Xue, L. Ma, S. Feng, M. Wan, F. Wang, C. Mao, Manganese phosphate self-assembled nanoparticle surface and its application for superoxide anion detection, Sci. Rep. 6 (2016) 28989.
[26] Y. Wang, D. Wang, L.H. Sun, P. Xue, M.Q. Wang, Z. Lu, F. Wang, Q. Xia, M.W. Xu, S.J. Bao, Constructing high effective nano-$Mn_3(PO_4)_2$-chitosan in situ electrochemical detection interface for superoxide anions released from living cell, Biosens. Bioelectron. 133 (2019) 133–140.
[27] L. Gao, J. Xie, X. Ma, M. Li, L. Yu, DNA@Mn3(PO4)2 nanoparticles supported with graphene oxide as photoelectrodes for photoeletrocatalysis, Nanoscale Res. Lett. 12 (2017) 17.
[28] A.M. Puziy, O.I. Poddubnaya, A.M. Ziatdinov, On the chemical structure of phosphorus compounds in phosphoric acid-activated carbon, Appl. Surf. Sci. 252 (2006) 8036–8038.
[29] X. Ma, W. Hu, C. Guo, L. Yu, L. Gao, J. Xie, C.M. Li, DNA-templated biomimetic enzyme sheets on carbon nanotubes to sensitively in situ detect superoxide anions released from cells, Adv. Funct. Mater. 24 (2014) 5897–5903.
[30] Y. Luo, Y. Tian, Q. Rui, Electrochemical assay of superoxide based on biomimetic enzyme at highly conductive TiO_2 nanoneedles: from principle to applications in living cells, Chem. Commun. (2009) 3014–3016.
[31] H. Wei, T. Shang, T. Wu, G. Liu, L. Ding, X. Liu, Construction of an ultrasensitive non-enzymatic sensor to investigate the dynamic process of superoxide anion release from living cells, Biosens. Bioelectron. 100 (2018) 8–15.
[32] J.Y. Yu, Z.H. Zheng, Y.O. Son, X. Shi, Y.O. Jang, J.C. Lee, Mycotoxin zearalenone induces AIF- and ROS-mediated cell death through p53- and MAPK-dependent signaling pathways in RAW264.7 macrophages, Toxicol. In Vitro 25 (2011) 1654–1663.
[33] R. You, H. Sun, Y. Yu, Z. Lin, M. Qin, Y. Liu, Time-dependent hormesis of chemical mixtures: a case study on sulfa antibiotics and a quorum-sensing inhibitor of Vibrio fischeri, Environ. Toxicol. Pharmacol. 41 (2016) 45–53.
[34] Q. Gao, J. Wang, L. Ren, Y. Cheng, Z. Lin, X.G. Li, H. Sun, Investigations on the influence of energy source on time-dependent hormesis: a case study of sulfadoxine to Aliivibrio fischeri in different cultivation systems, Sci. Total Environ. 775 (2021) 145877.
[35] E.O. da Silva, A.P.F.L. Bracarense, I.P. Oswald, Mycotoxins and oxidative stress: where are we?, World Mycotoxin J 11 (1) (2018) 113–134.
[36] T. Lajqi, M. Stojiljkovic, R. Wetzker, Toxin-induced hormesis may restrain aging, Biogerontology 20 (2019) 571–581.
[37] F.X. Hu, Y.J. Kang, F. Du, L. Zhu, Y.H. Xue, T. Chen, L.M. Dai, C.M. Li, Living cells directly growing on a DNA/$Mn_3(PO_4)_2$-immobilized and vertically aligned CNT array as a free-standing hybrid film for highly sensitive in situ detection of released superoxide anions, Adv. Funct. Mater. 25 (2015) 5924–5932.
[38] X. Liu, M. Ran, G. Liu, X. Liu, Z. Xue, X. Lu, A sensitively non-enzymatic amperometric sensor and its application in living cell superoxide anion radical detection, Talanta 186 (2018) 248–255.
[39] H. Zhang, X. Cai, H. Zhao, W. Sun, Z. Wang, M. Lan, Enzyme-free electrochemical sensor based on ZIF-67 for the detection of superoxide anion radical released from SK-BR-3 cells, J. Electroanal. Chem. 855 (2019) 113653.
[40] C.H. Foyer, H. Lopez-Delgado, J.F. Dat, I.M. Scott, Hydrogen peroxide- and glutathione-associated mechanisms of acclimatory stress tolerance and signalling, Physiol. Plant. 100 (1997) 241–254.
[41] L.L. Ji, C. Kang, Y. Zhang, Exercise-induced hormesis and skeletal muscle health, Free Radic. Biol. Med. 98 (2016) 113–122.
[42] A. Galano, Carbon nanotubes: promising agents against free radicals, Nanoscale 2 (2010) 373–380.
[43] E.L. Mills, B. Kelly, A. Logan, A.S.H. Costa, M. Varma, C.E. Bryant, P. Tourlomousis, J.H.M. Dabritz, E. Gottlieb, I. Latorre, S.C. Corr, G. McManus, D. Ryan, H.T. Jacobs, M. Szibor, R.J. Xavier, T. Braun, C. Frezza, M.P. Murphy, L.a. O'Neill, Succinate dehydrogenase supports metabolic repurposing of mitochondria to drive inflammatory macrophages, Cell 167 (2016) 457–470 e413.
[44] J. Kamarauskaite, R. Baniene, D. Trumbeckas, A. Strazdauskas, S. Trumbeckaite, Increased succinate accumulation induces ROS generation in in vivo ischemia/reperfusion-affected rat kidney mitochondria, Biomed. Res. Int. 2020 (2020) 8855585.
[45] D. Jardim-Messeder, A. Caverzan, R. Rauber, E. de Souza Ferreira, M. Margis-Pinheiro, A. Galina, Succinate dehydrogenase (mitochondrial complex II) is a source of reactive oxygen species in plants and regulates development and stress responses, New Phytol. 208 (2015) 776–789.